Article:
Lu, H., Wang, H., Liu, Y. et al. (2020) Substance transfer behavior controlled by droplet internal circulation. Chemical Engineering Journal, 393. 124657. ISSN: 1385-8947

https://doi.org/10.1016/j.cej.2020.124657

Journal Pre-proofs

Substance transfer behavior controlled by droplet internal circulation

Hao Lu, Hualin Wang, Yiqian Liu, Meihong Wang, Jun Hu, Qiang Yang

PII: S1385-8947(20)30648-3
DOI: https://doi.org/10.1016/j.cej.2020.124657
Reference: CEJ 124657

To appear in: *Chemical Engineering Journal*

Received Date: 13 October 2019
Revised Date: 1 February 2020
Accepted Date: 4 March 2020

Please cite this article as: H. Lu, H. Wang, Y. Liu, M. Wang, J. Hu, Q. Yang, Substance transfer behavior controlled by droplet internal circulation, *Chemical Engineering Journal* (2020), doi: https://doi.org/10.1016/j.cej.2020.124657

Substance transfer behavior controlled by droplet internal circulation

Hao Lu[a], Hualin Wang[a], Yiqian Liu[a], Meihong Wang[b], Jun Hu[c], Qiang Yang[a,]*

[a] State Environmental Protection Key Laboratory of Environmental Risk Assessment and Control on Chemical Process, East China University of Science and Technology, Shanghai 200237, P.R. China

[b] Department of Chemical and Biological Engineering, The University of Sheffield, 5 Mappin Street, Sheffield, S1 3JD, UK

[c] School of Chemistry and Molecular Engineering, East China University of Science and Technology, Shanghai 200237, P.R. China

ABSTRACT

Internal flow can be induced by the external flow around a droplet. In the present work, the three-dimensional flow pattern and dynamic characteristics of the internal vortex of adhered droplet were demonstrated firstly, and then the substance transfer behavior within the droplet dominated by the internal circulation was revealed by adopting two systems, namely fluorescence reaction and suspended particle capture, and combining with an interface reaction model developed. It was found that the internal circulation could not only transfer the reactants from the inside onto the surface of the droplet quickly, but also carry the particles captured on

*Corresponding author.

E-mail address: qyang@ecust.edu.cn (Q. Yang).

the droplet surface into the vortex core rapidly in a vortex manner, which could improve the reaction rate and control the capture process. This work uniquely demonstrates fundamental insights into the internal flow pattern of adhered droplet and promotes an understanding of the multiphase droplet-based mass transfer mechanism and particle capture process.

Keywords: droplet internal circulation; mass transfer; interface reaction; particle capture; vortex

1. Introduction

To disentangle the complexity of mass transfer and reaction processes in multiphase polydispersed systems, it is particularly useful to reduce the complexity of swarm systems to single droplets because droplets are the smallest mass transfer unit [1]. For this reason, droplet-related research has always been an important research direction in the fields of chemical engineering, mechanical design, etc., especially in the processes of mixing, extraction, adsorption, evaporation, reaction, etc. In fact, a variety of phenomena in daily life are related to the internal flows of droplets, such as the internal vortex of free-falling raindrops generated by the drag of air hydrodynamics [1,2], and the well-known Marangoni flow in evaporating droplets caused by the surface tension gradient [3,4]. Fluid dynamics and mass transfer are inseparable. To understand and control the mass transfer mechanism of a droplet, it is necessary to first study the flow pattern inside the droplet. Based on microfluidic technology, extensive investigations, both experimental and numerical, have been conducted on the internal flow of a droplet during its formation and the subsequent moving stages in microchannels [5-8]. Micro-

PIV (Particle Image Velocimetry) technology is the main experimental method used to explore the droplet's internal flow field [6-13]; and numerical methods include the CFD method [14-19], Lattice Boltzmann method [20,21], immersed-boundary [22], etc.; and the research systems include absorption [23], extraction [24-26], mixing [27,28], reaction [29,30], condensation [31], evaporation [32,33], functional materials [34,35] and double emulsion droplet [36], etc. These reported studies reveal the existence of vortices within the droplet are crucial for enhancing mixing and improving the mass transfer across the interface. There are also a lot of adhered droplets on the surface of the medium in multiphase flow and reaction systems, and the interior flow of these adhered droplets may be induced by the external flow. However, for an adhered droplet no comprehensive reports have been made so far on what the internal flow pattern is, how the external flow and droplet properties affect its internal flow, or how well the internal flow promotes the mass transfer performance.

The motivation for the present work was to obtain a comprehensive understanding of the internal vortices of an adhered droplet, in order to further improve the understanding of the internal vortex's effect on the mass transfer and particle capture processes, and to provide intuitive and visible test results and a quantitative characterization. Experimental tests were performed to visually demonstrate the internal flow behavior. Additionally, according to our previous research on the incipient motion condition of an adhered droplet [37], we designed a user-defined function (UDF_1) to avoid the deficiency of the existing CFD wall adhesion model, so that the simulated interior flow pattern was consistent with the experimental observation, and the effects of surface wettability, interface property and fluid property on the internal flow were studied by the numerical method. Furthermore, a fluorescence reaction

experiment was designed to demonstrate the intensification effect of the internal circulation on the droplet reaction, and we also developed an interface reaction model via the UDF_2 to reveal the influence of the internal circulation on the reaction process. In addition, we also designed a particle capture experiment, which showed the migration pattern and accumulation process of the captured particles controlled by the internal vortices.

2. Experimental and numerical methods

2.1. Experimental procedure for internal circulation flow

Water was used as the continuous phase shear fluid, a silicone oil droplet was used as the dispersed phase droplet adhered to the solid substrate surface, and the internal circulation behavior of the adhered oil droplet was studied. A micro-droplet of water was injected into the oil droplet, and the internal flow field of the oil droplet could be reflected by the movement of the micro-droplet, so the micro-droplet acted as a tracer particle. For more details on the experimental setup (Fig. S1(a)), materials, test video (Video S1), and image processing (Fig. S2), see the supplementary material.

2.2. Numerical method for internal circulation flow

The volume of fluid method (VOF) based on Computational Fluid Dynamics (CFD) was adopted to simulate the droplet's internal flow. Since the existing VOF wall adhesion boundary could not impose an adhesion force to the droplet, we designed a UDF_1 to fix the droplet onto the surface, so that the simulation result was consistent with the experimental observation. For more details about the standard VOF method, the content and efficacy of the UDF_1 (Fig. S3),

computational domain (Fig. S4), variables (Table S1), and simulated video (Video S2), see the supplementary material.

2.3. Experimental procedure for the fluorescence reaction

The aqueous phase consisted of H_2O_2 and deionized water, while the oil phase consisted of CPPO, DBP and a fluorescent agent. The induction periods required for reaching a specific amount of reaction (the initial luminous time) were measured under various aqueous phase flow rates, and they could be used to characterize the average reaction rates under different internal circulation strengths. For more details on the experimental setup (Fig. S1(c)), materials, fluorescence mechanism, definition of initial luminous time, and video of the fluorescence process (Video S3), see the supplementary material.

2.4. Numerical method for interface reaction

The coupling method of VOF and Species Transport based on CFD was adopted to simulate the droplet interface reaction. We simplified the fluorescence reaction equation and assumed that the reaction only occurred at the interface, and the reaction rate was only related to the concentration of the reactants at the interfacial grid. Since the existing CFD model could not handle the interface reaction, we developed a UDF_2 to implement the interface reaction. For more details about the content of the UDF_2, simplification and assumption, and parameter setting (Table S2), see the supplementary material.

2.5. Experimental procedure for particle capture

A basic copper carbonate suspension formed by the reaction of copper sulfate and the

sodium hydrogen carbonate was prepared as the continuous phase suspension, and silicone oil droplets were used as the adhered droplets to capture the suspended particles. The phenomena of particle capture and migration under various droplet viscosities and flow rates were observed. For more details on the experimental setup, materials, and video of the particle capture process (Video S4), see the supplementary material.

3. Results and discussion

3.1 Internal circulation phenomenon within an adhered droplet

Driven by external water flow, a steady, periodic, repeated rotational motion occurs within the oil droplet (Video S1). For a single micro-droplet rotation trajectory, the velocity near the windward side is relatively fast, while the velocity near the leeward side and the bottom is relatively slow, and the velocity declines along the rotating streamline (Fig. 1(c-h)). For multiple micro-droplet rotation trajectories at different streamline positions, they rotate around the same center; the closer to the center, the slower the movement (Fig. 1(b)), indicating that there is a low-velocity center of rotation, which can be considered as the vortex core. Therefore, on the whole, there are three low-velocity regions, namely, the vortex core region, the lower region of the leeward side, and the bottom region, while the velocity on the windward side is the fastest, then it declines along both the circumferential and the radial directions (Fig. 1(a-b)).

Causes of the vortex and its velocity distribution: there is a large velocity slip between the adhered droplet and the external flow, which induces the flow inside the droplet. Since the external flow field is stable and laminar, it has a stable and uniform shear driving action, thus

forming a stable internal circulation flow within the droplet. The rotation velocity inside the droplet is much less than the velocity of the external flow. For example (Fig. 1(g), the average velocity of the external flow was 0.054 m/s, which was about 143 times of the average velocity of the rotating micro-droplet (0.000377 m/s) within the oil droplet. The velocity gradient between the upper interface region of the windward and the external water flow is the largest, and the driving force comes from the shear force on this region between the two fluid phases. We simply consider that the shear force's direction is tangent to the interface, which is the power source driving the internal flow within the droplet. Therefore, under the action of the shear force, tangential (circumferential) velocity is generated on the upper interface region of the windward side. Due to flow resistance, the velocity declines along the circumferential streamline direction towards the rear of the leeward side. In addition, from the interface to inside, in the radial direction perpendicular to the streamline, the inner layer of the adjacent fluid is subject to the laminar shear force of the outer layer, which also generates circumferential rotation velocity. The attenuation mode of velocity along the radial direction is laminar shear attenuation, which results in the formation of an inner low-velocity rotating vortex core.

One way of accelerating the internal circulation is to raise the external driving force, and the other is to reduce the internal friction resistance within the droplet. When the external flow rate rises, the velocity gradient at the two-phase interface increases, resulting in an increase in the driving force. As the droplet viscosity decreases, the internal frictional resistance decreases, so the circulating flow inside the droplet is enhanced (Fig. 1(c-h)). For droplet viscosity_400 cP, as the increase of the external flow rate from 0.027 m/s to 0.108 m/s, the average velocity

of the micro-droplets was 0.000092 m/s (Fig. 1(c)), 0.00017 m/s (Fig. 1(d)) and 0.000295 m/s (Fig. 1(e)), respectively. However, when the droplet viscosity decreased to 90 cP, the average velocity of the corresponding micro-droplets increased to 0.000205 m/s (Fig. 1(f)), 0.000377 m/s (Fig. 1(g)) and 0.000788 m/s (Fig. 1(h)), respectively.

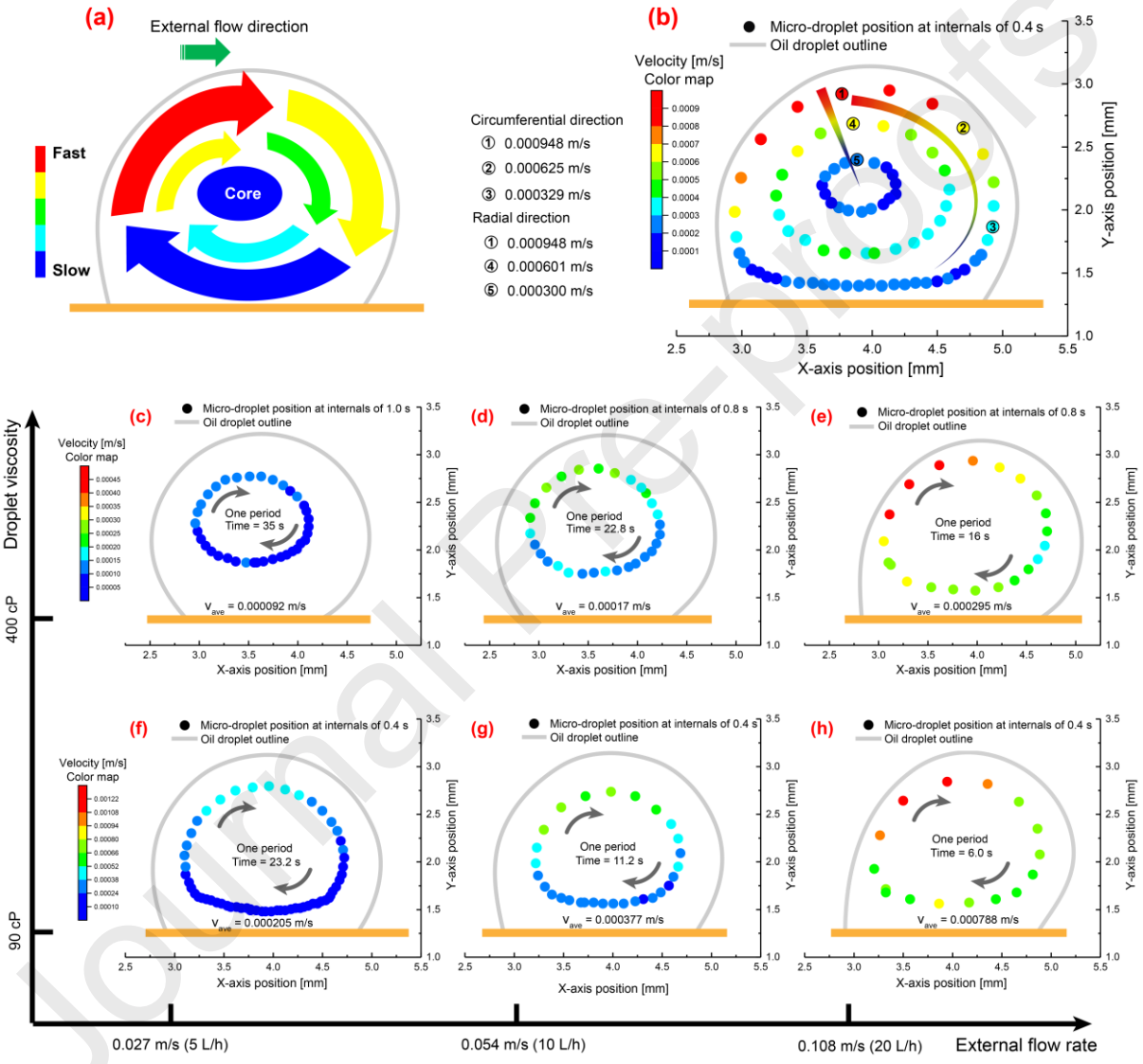

Fig. 1. Internal circulation and velocity distribution. (a) The whole droplet is rotated, and the center of rotation is a low-velocity vortex core region. The velocity on the windward side is the fastest, and then it attenuates in both the circumferential and radial directions. (b) The velocity distribution at different streamline positions demonstrates the mode of velocity attenuation.

The trajectory and velocity distribution of the micro-droplet at three different streamline positions within one rotation period, one rotation period from inner to outer was 7.2 s, 8.6 s, and 15.8 s, under the test conditions: viscosity_90 cP, flow rate_0.054 m/s. (c-e) High viscosity and various flow rate. As the external flow rate increases, the micro-droplet's rotation accelerates. (f-h) Low viscosity and various flow rate. Compared with (c-e), the viscosity is reduced and the micro-droplet rotation velocity is increased.

3.2 Flow pattern and dynamic characteristics

The experimental test can obtain only the motion trajectory of the micro-droplet on the projection plane, while the simulation method can be used to obtain the three-dimensional flow field within the oil droplet, such as the shape, position and velocity distribution of the entire vortex (Fig. 2). The average velocity of the external flow is much larger than the average velocity within the droplet (Fig. 2(b)), and the external flow has the maximum velocity gradient in the area close to the interface of the upper windward side (Fig. 2(a-b)), and the shear force from this area drives the rotation of the vortex. For the vortex, the velocity presents a circulation distribution of fast-slow-fast along the direction of rotation, and the velocity decreases toward the vortex core (Fig. 2(d)). The vortex core is almost stationary, acting like an arch bridge with the entire vortex rotates around it (Fig. 2(f)). The lower region of the leeward side is located outside the overall vortex (Fig. 2(e)), and it is also almost stationary. The flow pattern obtained by this method is consistent with the internal circulation phenomenon observed by experiment. Moreover, the relative velocity distribution on the streamline is also consistent with that on the rotation trajectory of the micro-droplet tested (In Fig. S5, the simulated and tested results of

velocity distribution were compared in detail). Therefore, this modified simulation method can be used to study the dynamics of circulation motion within the droplet.

By slicing the droplet, the velocity distribution on different planes can be observed (Fig. S6(a-c)). The area-weighted average of the velocity on the planes will gradually decrease as the planes move away from the symmetry plane (Fig. S7(a)). From the perspective of the swirling strength (its value represents the strength of the swirling motion around the local center, which is related to the change in the velocity gradient), only the region between the upper area of the windward side and the vortex core has a relatively large vortex strength (Fig. S6(d-e)), and it is this region that drives the motion of the entire vortex. The swirling strengths in the remaining regions are quite small, indicating that the velocity gradient changes in the remaining regions are quite small. The effects of various parameters on the strength of the internal circulation are quantitatively compared (Fig. S7(b-d)), characterized by the volume-weighted average values of the velocity and swirling strength. The results show that the droplet viscosity has the most obvious effect on the strength of the internal circulation, while the interfacial tension and droplet volume have little effect. The increase in both the contact angle and external flow rate can make the droplet obtain a more external shear force, which then strengthens the internal flow. For example, the volume-weighted average velocity under the control group condition (viscosity_100 cP, flow rate_0.054 m/s) was 0.000595 m/s; for the effect of viscosity, when the viscosity decreased to 10 cP, it rose to 0.00449 m/s (7.55 times), while when the viscosity increased to 500 cP, it decreased to 0.000166 m/s (0.28 times); for the effect of the external flow rate, when the external flow rate decreased to 0.027 m/s, it decreased to 0.00023 m/s (0.39 times), while when the external flow rate increased to 0.108 m/s, it rose to 0.00147

m/s (2.47 times).

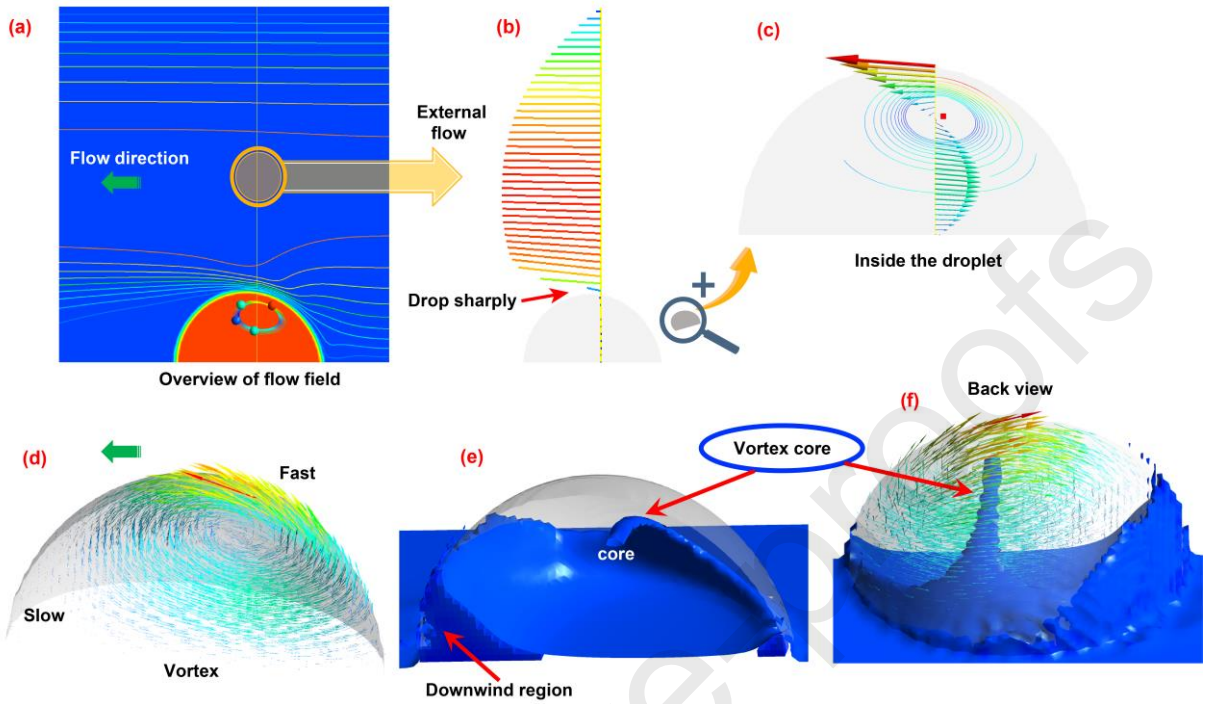

Fig. 2. Comprehensive flow pattern. (a) Overall external flow field in the channel. In the channel, the external flow field is laminar, and the adhered droplet acts as an obstacle. When the external fluid passes around the droplet, it has the maximum velocity gradient (streamlines are the densest) in the area close to the upper part of the windward side, while it is almost stationary in the area behind the leeward side of the droplet. (b) The velocity distribution on a vertical line (the yellow line from (a)) passing through the droplet. The length and direction of the line represent the relative magnitude and direction of the velocity. The external flow velocity has a parabolic distribution, and it drops sharply when approaching the droplet interface. Compared with the external flow velocity, the velocity within the droplet is too small, so that the velocity line inside the droplet is barely visible. (c) Local relative velocity distribution inside the droplet. Local magnification of the droplet (from (b)) shows the local

relative velocity distribution inside the droplet. Along the vertical yellow line, the velocity distribution is as follows: the maximum at the interface decays downward to zero at the center of the vortex, then in a reversed direction it increases first and then decreases, and finally declines to zero at the bottom surface. (d) Three-dimensional local velocity vector. The three-dimensional velocity vector in half of the droplet shows the overall position of the entire vortex and the relative velocity distribution. (e) Low-velocity regions. The blue region is the low-velocity region where the velocity value is no more than 0.0002 m/s, including the vortex core region, bottom adhered region, and lower region of the leeward side, which are almost stationary. (f) Velocity profile combined (d) and (e). (Data from the simulation under control group conditions, Table S1)

3.3 Enhance droplet reaction

How does the internal circulation affect the droplet reaction? We designed the fluorescence reaction system to reveal this from both experimental test and the theoretical mechanism. The above two parts of the study show that when the physical properties of the oil droplet remain unchanged, the strength of the internal circulation can be raised by increasing the external flow rate. Therefore, we test the induction periods (time period required for reaching a specific amount of reaction, Fig. 3(a)) under various aqueous phase flow rates, and consider that they reflect the average reaction rate under different internal circulation strengths. When the aqueous phase flow rate was 0 m/s (stationary state), it was believed that there was no internal circulation in this case and the reaction was only promoted by diffusion (ignoring the convection caused by the reaction itself), so the induction period required 65 min. During

the aqueous phase flow, the internal circulation occurs and the reaction rate is accelerated under the dual action of the internal circulation and diffusion. The larger the strength of the internal circulation, the faster the reaction rate is, so it requires shorter time to reach the initial luminance. Tests (Fig. 3(c)) showed that it took 15.5 min when the flow rate was 0.035 m/s (corresponding to the volume-weight average velocity of internal circulation was about 0.00256 m/s), and the average reaction rate is 4.2 times that of the stationary state, while it only took 6 min when the flow rate reached 0.108 m/s (corresponding to the volume-weight average velocity of internal circulation was about 0.011 m/s), and the average reaction rate was 10.8 times that of the stationary state. Therefore, the fluorescence experiment effectively confirmed the enhanced effect of the internal circulation on the droplet reaction.

Furthermore, we developed the interface reaction model to reveal the action mechanism of internal circulation on enhancing droplet reaction process. It is believed that the reaction only occurs at the interface, so both diffusion caused by the concentration gradient and convection caused by the internal circulation bring the reactants inside the droplet to the interface to sustain the reaction. The overall reaction rate can be characterized by the reduction rate of the reactant CPPO. The area average mass fraction of CPPO decreases with the reaction time. Compared with the stationary state (aqueous phase flow rate 0 m/s), the mass fraction of CPPO decreased faster in the case of 0. 1 m/s, and the difference between the two reduction rate curves was the effect of the internal circulation (Fig. 3(d)). CPPO inside the droplet was rapidly carried to the interface by the internal circulation to supplement the CPPO consumed by the interface reaction, and the internal circulation reduced the concentration gradient from the center to the interface and brought the CPPO concentration within the entire droplet evenly

(Fig. 3(f)). It could be seen from the CPPO mass fraction contour (Fig. 3(d-f)): in the case of 0 m/s, the CPPO mass transfer was controlled by the radial diffusion driven by the concentration gradient, where the highest concentration was located in the droplet center (bottom center) and spread outward in the radial direction, and the mass transfer rate was relatively low. However, in the case of 0.1 m/s, the CPPO mass transfer was controlled by the coupling of diffusion and the internal circulation, and appeared to be dominated by the internal circulation, where the highest concentration migrated from the droplet center to the vortex center, and the mass transfer rate was relatively high.

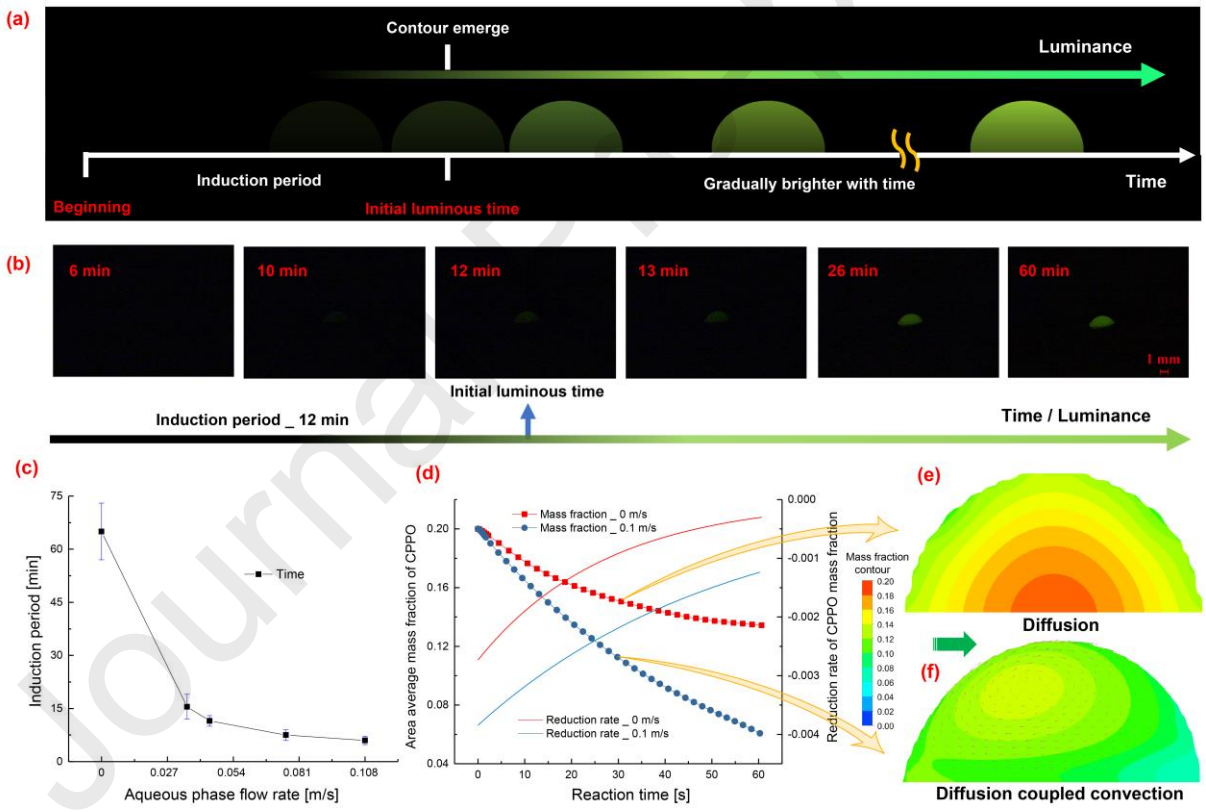

Fig. 3. Influence of the internal circulation on mass transfer. (a) Schematic diagram of the fluorescence process. In the beginning, the entire scene is dark, and the droplet contour cannot be observed. As the reaction progresses, the droplet contour gradually emerges and becomes

brighter. We define the time at which the vague contour of the droplet just emerges (vague contour emerges, only when the total amount of the reaction accumulates to a certain amount can the vague contour of the droplet emerge) as the initial luminous time, and the interval between the beginning and the initial luminous time is the induction period. Note that we do not consider the subsequent changes after the induction period here. (b) Image capture of the fluorescence process (Video S3). Images captured at different times during the experiment corresponding to the schematic diagram in (a), where the vague contour of the droplet emerged at 12 min. (c) Experimental test of the induction period under various aqueous phase flow rates. (d) The change of CPPO concentration (mass fraction) and CPPO reduction rate obtained through the interface reaction model. The area average mass fraction of CPPO decreased with time in the cases of the aqueous phase flow rate of 0 m/s and 0.1 m/s (velocity-inlet boundary condition). The reduction rate curve is the derivative of the mass fraction fitting curve (single exponential attenuation fitting curve, R^2=0.999). The difference between the two reduction rate curves is the effect caused by the internal circulation. (e) Diffusion. CPPO mass fraction contour at 30 s in the case of 0 m/s. (f) Diffusion coupled convection. CPPO mass fraction contour together with velocity vector at 30 s in the case of 0.1 m/s.

3.4 Vortex migration on particle capture.

To understand the role of the internal circulation in particle capture, we prepared a basic copper carbonate suspension to observe the process of particle capture by the droplet. A very interesting phenomenon of the vortex particle migration and accumulation process was demonstrated (Video S4). There are two symmetric vortices inside the droplet (Fig. 4(a)) and

the center of each vortex is a low-velocity rotating vortex core, so the macroscopic motion phenomenon of captured particles observed is consistent with the flow field obtained by the above study (Fig. 2(f)). For each vortex, the particles captured from the droplet surface or the vortex edge will be continuously carried into the vortex core by internal circulation, and all captured particles will gradually converge inward to the vortex core region and rotate around the vortex center (Fig. 4(b-d)). The total amount of captured particles increases with the flow time, and the area occupied by the particles gradually expands radially outward from the vortex center to the entire droplet. Eventually, when the entire surface of the droplet is wrapped by the particles (Fig. 4(e-g)), it seems that the droplet is saturated with particles, which prevents contact between the droplet surface and the external fluid. From observation, the internal rotation of the droplet seems to have stopped. The results show that the internal circulation controls the migration and accumulation of particles in the process of particle capture.

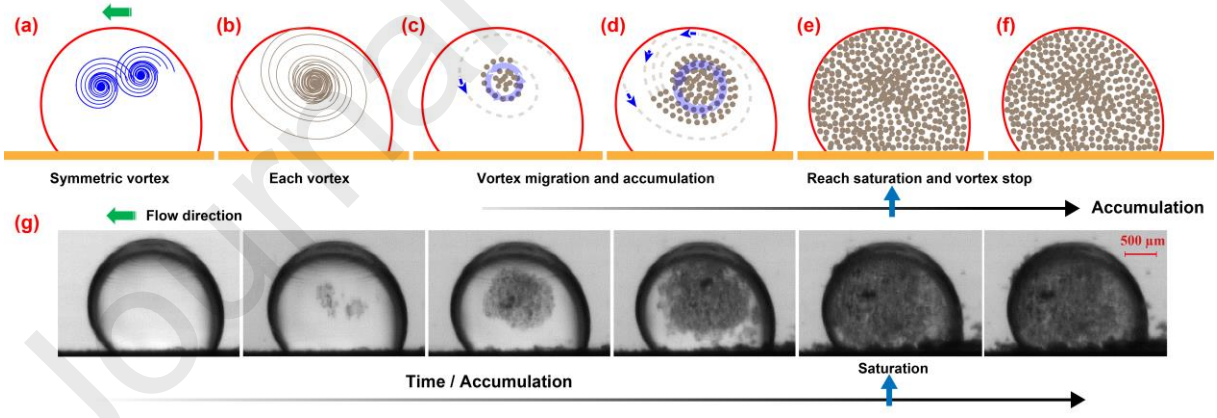

Fig. 4. Influence of internal circulation on particle capture process. (a) Symmetric vortex. There are two symmetric vortices inside the droplet, so it can be assumed that the droplet could be divided into two symmetric parts. (b) Particle migration. The particles captured from the vortex edge will be continuously carried into the vortex core by internal circulation. (c-e)

Accumulation. The accumulation of particles in the droplet gradually increases with the flow time until reaching saturation. (f) Saturation. After reaching the saturated state, from a visual observation the droplet is completely wrapped by the captured particles, and the interior vortices seem to have stopped. (g) Images of particle accumulation process with flow time. (under the test condition: viscosity_90 cP, flow rate_0.081 m/s, volume_6 μL)

4. Conclusions

In summary, the interesting phenomenon of the internal circulation and the basic pattern of the three-dimensional vortex within the adhered droplet have been demonstrated intuitively, and the important role of the internal circulation in the mass transfer and particle capture process has been revealed. The internal circulation can not only transfer the reactants from the inside onto the surface of the droplet quickly, but also carry the particles captured on the droplet surface into the vortex core rapidly in a vortex manner, which can improve the reaction rate and control the capture process. We envision that the results and insights obtained from the present work will be useful in understanding other processes involving droplets, especially when systems with significant liquid-solid adhesion are involved.

Acknowledgments

This work is supported by the National Natural Science Foundation of China (Grant NO. 51678238, 51722806) and National Key Research and Development Project (Grant NO. 2019YFA0705800).

References

[1] M. Wegener, N. Paul, M. Kraume, Fluid dynamics and mass transfer at single droplets in liquid/liquid systems, Int. J. Heat Mass Transfer 71 (2014) 475-495.

[2] B. LeClair, A. Hamielec, H. Pruppacher, W. Hall, A theoretical and experimental study of the internal circulation in water drops falling at terminal velocity in air, J. Atmos. Sci. 29 (1972) 728-740.

[3] A. Al-Sharafi, H. Ali, B.S. Yilbas, A.Z. Sahin, N. Al-Aqeeli, F. Al-Sulaiman, M. Khaled, Internal flow and heat transfer in a droplet located on a superhydrophobic surface, Int. J. Therm. Sci. 121 (2017) 213-227.

[4] D.K. Mandal, S. Bakshi, Internal circulation in a single droplet evaporating in a closed chamber, Int. J. Multiphase Flow 42 (2012) 42-51.

[5] W. Gao, M. Liu, S. Chen, C. Zhang, Y. Zhao, Droplet microfluidics with gravity-driven overflow system, Chem. Eng. J. 362 (2019) 169-175.

[6] Q.Q. Xiong, Z. Chen, S.W. Li, Y.D. Wang, J.H. Xu, Micro-PIV measurement and CFD simulation of flow field and swirling strength during droplet formation process in a coaxial microchannel, Chem. Eng. Sci. 185 (2018) 157-167.

[7] G. Liu, X. Wang, K. Wang, C.P. Tostado, G. Luo, Effect of surface wettability on internal velocity profile during droplet formation process in microfluidic devices, Int. J. Multiphase Flow 80 (2016) 188-193.

[8] X. Wang, G. Liu, K. Wang, G. Luo, Measurement of internal flow field during droplet formation process accompanied with mass transfer, Microfluid. Nanofluid. 19 (2015) 757-766.

[9] G. Minor, N. Djilali, D. Sinton, P. Oshkai, Flow within a water droplet subjected to an air

stream in a hydrophobic microchannel, Fluid Dyn. Res. 41 (2009) 045506.

[10] M. Oishi, H. Kinoshita, T. Fujii, M. Oshima, Simultaneous measurement of internal and surrounding flows of a moving droplet using multicolour confocal micro-particle image velocimetry (micro-PIV), Meas. Sci. Technol. 22 (2011) 105401.

[11] M.R. Duxenneuner, P. Fischer, E.J. Windhab, J.J. Cooper-White, Simultaneous visualization of the flow inside and around droplets generated in microchannels, Microfluid. Nanofluid. 16 (2014) 743-755.

[12] F. Sarrazin, K. Loubiere, L. Prat, C. Gourdon, T. Bonometti, J. Magnaudet, Experimental and numerical study of droplets hydrodynamics in microchannels, AIChE J. 52 (2006) 4061-4070.

[13] H. Kinoshita, S. Kaneda, T. Fujii, M. Oshima, Three-dimensional measurement and visualization of internal flow of a moving droplet using confocal micro-PIV, Lab Chip 7 (2007) 338-346.

[14] G. Yang, A. Terzis, I. Zarikos, S.M. Hassanizadeh, B. Weigand, R. Helmig, Internal flow patterns of a droplet pinned to the hydrophobic surfaces of a confined microchannel using micro-PIV and VOF simulations, Chem. Eng. J. 370 (2019) 444-454.

[15] Z.G. Feng, E.E. Michaelides, Drag coefficients of viscous spheres at intermediate and high Reynolds numbers, J. Fluids Eng. 123 (2001) 841-849.

[16] S. Burghoff, E.Y. Kenig, A CFD model for mass transfer and interfacial phenomena on single droplets, AIChE J. 52 (2006) 4071-4078.

[17] S.G. Sontti, A. Atta, CFD analysis of microfluidic droplet formation in non-Newtonian liquid, Chem. Eng. J. 330 (2017) 245-261.

[18] C.A. Edelmann, P.C. Le Clercq, B. Noll, Numerical investigation of different modes of internal circulation in spherical drops: fluid dynamics and mass/heat transfer, Int. J. Multiphase Flow 95 (2017) 54-70.

[19] K. Sultana, K. Pope, L. Lam, Y. Muzychka, Phase change and droplet dynamics for a free falling water droplet, Int. J. Heat Mass Transfer 115 (2017) 461-470.

[20] B. Maneshian, K. Javadi, M.T. Rahni, R. Miller, Droplet Dynamics in Rotating Flows, Adv. Colloid Interface Sci. 236 (2016) 63-82.

[21] S. Zhao, A. Riaud, G. Luo, Y. Jin, Y. Cheng, Simulation of liquid mixing inside micro-droplets by a lattice Boltzmann method, Chem. Eng. Sci. 131 (2015) 118-128.

[22] B. Yin, H. Luo, Numerical simulation of drops inside an asymmetric microchannel with protrusions, Comput. Fluids 82 (2013) 14-28.

[23] Z. Wang, T. Guo, L. Tian, Q. Xu, S. Zhan, J. Tu, Numerical simulation on circulation flow and mass transfer inside atmospheric water drops, Appl. Therm. Eng. 118 (2017) 765-772.

[24] P. Mary, V. Studer, P. Tabeling, Microfluidic droplet-based liquid-liquid extraction, Anal. Chem. 80 (2008) 2680-2687.

[25] D. Das, S. Duraiswamy, Z. Yi, V. Chan, C. Yang, Continuous droplet-based liquid-liquid extraction of phenol from oil, Sep. Sci. Technol. 50 (2015) 1023-1029.

[26] H. Zhang, H. Wang, X. Luo, D.Y. Leung, Q. Pang, H. Xu, L. Zhang, J. Xuan, Toward a mechanistic understanding of microfluidic droplet-based extraction and separation of lanthanides, Chem. Eng. J. 356 (2019) 673-679.

[27] N. Lebaz, N. Sheibat-Othman, A population balance model for the prediction of breakage of emulsion droplets in SMX+ static mixers, Chem. Eng. J. 361 (2019) 625-634.

[28] L. Bai, Y. Fu, M. Yao, Y. Cheng, Enhancement of mixing inside ionic liquid droplets through various micro-channels design, Chem. Eng. J. 332 (2018) 537-547.

[29] J. Xu, J. Tan, S. Li, G. Luo, Enhancement of mass transfer performance of liquid-liquid system by droplet flow in microchannels, Chem. Eng. J. 141 (2008) 242-249.

[30] K. Wang, L. Li, P. Xie, G. Luo, Liquid-liquid microflow reaction engineering, React. Chem. Eng. 2 (2017) 611-627.

[31] Z. Yang, X.C. Ma, Y.Y. Duan, Y. Chen, Internal flow and heat transfer of a condensing water droplet in steam flow, Chem. Eng. Sci. 94 (2013) 54-59.

[32] M. He, H. Qiu, Internal flow patterns of an evaporating multicomponent droplet on a flat surface, Int. J. Therm. Sci. 100 (2016) 10-19.

[33] A. Saufi, R. Calabria, F. Chiariello, A. Frassoldati, A. Cuoci, T. Faravelli, P. Massoli, An experimental and CFD modeling study of suspended droplets evaporation in buoyancy driven convection, Chem. Eng. J. (2019) 122006.

[34] J. Wang, L.Y. Sun, M.H. Zou, W. Gao, C.H. Liu, L.R. Shang, Z.Z. Gu, Y.J. Zhao, Bioinspired shape-memory graphene film with tunable wettability, Sci. Adv. 3 (2017) e1700004.

[35] J. Wang, W. Gao, H. Zhang, M.H. Zou, Y.P. Chen, Y.J. Zhao, Programmable wettability on photocontrolled graphene film, Sci. Adv. 4 (2018) eaat7392.

[36] Y.P. Chen, X.D. Liu, M.S. Shi, Hydrodynamics of double emulsion droplet in shear flow, Appl. Phys. Lett. 102 (2013) 051609.

[37] H. Lu, X. Xu, L.S. Xie, H.L. Wang, G.N. Sun, Q. Yang, Deformation and crawling of oil drop on solid substrates by shearing liquid, Chem. Eng. Sci. 195 (2019) 720-729.

Supplementary Figure Captions

Fig. S1. Experimental setup and image capture. (a) Flow diagram for the internal circulation test. Pump provides the fluid loop power, and the valves and flowmeter control and display flow rate, respectively; transparent channel (inner size 400 mm*7.5 mm*7.5 mm) with pasted substrate (400 mm*5 mm*1 mm) is used for the shooting channel; the syringe injects the oil droplets, which adhere to the substrate surface, and then the micro-droplet of water for the tracer function is injected into the oil droplet; black and white cameras and a light source are used for shooting. (b) Image capture of the internal circulation. Images are captured at a frequency of 5 fps, and the continuous images show the periodic circular motion of the micro-droplet in the oil droplet. (c) Flow diagram for the fluorescence reaction and particle capture test. Manually loop the aqueous phase liquid from the low tank to the high tank, and the gravitational potential energy supports the fluid flow. A color camera and dark field are used to capture the fluorescent droplet. (d) Image capture of fluorescence process. At the beginning, the entire scene is dark, and the droplet contour cannot be observed. As the reaction progresses, the droplet contour gradually emerges and becomes brighter. Only when the total amount of the reaction accumulates to a certain amount can the vague contour of the droplet emerge, and the corresponding time is the initial luminous time. (e) Image capture of particle capture. It is observed that there are two symmetric vortices inside the droplet, and the particles captured from the surface gradually migrate towards the center of the vortex. With an increase in the flow time, the accumulation of particles in the droplet gradually increases until becoming saturated.

Fig. S2. Experimental procedure for internal circulation flow – Image processing. (a) Motion

trajectory and velocity distribution of the micro-droplet within one rotating period (the data comes from one period of subgraph(b)). The interval between adjacent locations is 0.2 s, and 6 s is required for one rotation period. On the whole, the velocity of the micro-droplet on the windward side is faster, while those on the leeward side and at the bottom are slower. The oil droplet outline comes from the coordinates of the outline position in the image. (b) The central position coordinates of the micro-droplet and its velocity at each moment during the test time (20 seconds here). The central position of the micro-droplet is read and interpolated with the positions at the adjacent moments to obtain the velocity at the position. Subgraph (a) can be made by taking one period from a few of continuous cycles in subgraph(b). (c) A sequence of images at intervals of 0.2 s within one rotating period, corresponding to subgraph(a) and 1.8 s-7.8 s of subgraph(b). We can see that the micro-droplet is rotating, and its position of 7.8 s backs to that of 1.8 s, continuously rotating. (under test conditions: viscosity_90 cP, static contact angle_111°, volume_6 μL, flow rate_0.108 m/s)

Fig. S3. Qualitative differences between adding and not adding the UDF_1. (a) Not adding the UDF_1, the velocity vector and streamlines move forward. Because the existing wall adhesion boundary cannot impose adhesion force to the droplet, the droplet slides forward without internal circulation, even under a small external flow rate. (b) Adding the UDF_1, the velocity vector and streamlines rotate. This phenomenon is consistent with experimental observation: when the external flow rate is below the critical flow rate required for the initial motion, the adhered droplet does not slide and internal circulation occurs.

Fig. S4. computational domain. (a) Geometry for numerical simulation. Except for the length,

the shape and size are the same as the experimental channel. The inner section of the channel is 7.5 mm*7.5 mm, and a substrate of 5*1 mm is attached onto the channel. The droplets adhere to the surface of the substrate. To reduce the computational cost, only the channel of 6 mm in length is considered. (b) Computational domain and grid. Due to the symmetry of the channel and droplet, half of the channel is taken as the computational domain. (c) Boundary conditions.

Fig. S5. Comparison between simulation and experiment. (a) or (Fig. 1(b)) Test under a low viscosity system. The trajectory and velocity distribution of the micro-droplet at three different streamline positions, under the test condition: viscosity_90 cP, flow rate_0.054 m/s, static contact angle_111°, droplet volume_6 μL. (b) The simulation result corresponding to the conditions of test (a). The velocity distribution on the three corresponding streamlines on the plane P_3.25 obtained by simulation. (c) or (Fig. 1(d)) Test under a high viscosity system. The trajectory and velocity distribution of the micro-droplet, under the test conditions: viscosity_400 cP, flow rate_0.054 m/s, static contact angle_133°, droplet volume_6 μL. (d) Simulation results corresponding to the conditions of test (c). The velocity distribution on the corresponding streamline on the plane P_3.25 obtained by simulation.

Fig. S6. Velocity and swirling strength distribution on planes. (a) Positions of the five planes. The leftmost plane is the symmetry plane, and these five parallel planes offset each other by 0.25 mm. (b) The local velocity distribution and the velocity vector on the five planes. (c) A magnified view of the streamline and local velocity vector on the P_3.25 plane. The vortex region is mainly above the black line. (d) The purple region is where the swirling strength is equal or more than 1 s^{-1}. The swirling strength is the imaginary part of the complex eigenvalues

of the velocity gradient tensor, and its value represents the strength of the swirling motion around the local center. The swirling strength is related to the change in the velocity gradient, which indicates that the change of the velocity gradient in the pink areas is large, while it is small in the blue area. (e) The local swirling strength distribution on the five planes. Only the region between the upper area of the windward side and the vortex core has a relatively large vortex strength. The maximum swirling strength appears at the upper area of windward side. (simulation under the control group conditions)

Fig. S7. Effects of various parameters on the strength of internal circulation. (a) The area-weighted average of the velocity on the planes. The area-weighted average of velocity on the plane will gradually decrease as the plane moves away from the symmetry. (b) The volume-weighted average of velocity. (c) The area-weighted average of swirling strength on planes. As the plane is far away from the symmetry, the average swirling strength of the plane first increases and then decreases. (d) The volume-weighted average of the swirling strength. The effects of various parameters on the volume-weighted average of the swirling strength and velocity show the same trend. On the whole, the interfacial tension and droplet volume have little effect on the weighted average of the swirling strength and velocity of the droplet, while the viscosity has the most obvious effect on them. Meanwhile, the increase in the contact angle and flow rate will also enhance the internal flow. (simulation under the conditions of Table S1)

Video S1. Internal circulation test _ two times

Video S2. Simulation animation of internal circulation

Video S3. Fluorescence reaction process _ eight times

Video S4. Particle capture process _ two times

Declaration of interests

☑ The authors declare that they have no known competing financial interests or personal relationships that could have appeared to influence the work reported in this paper.

☐The authors declare the following financial interests/personal relationships which may be considered as potential competing interests:

- Analyzed the fluid dynamics of droplet internal circulation
- Revealed the substance transfer behavior controlled by internal circulation
- Developed numerical methods for droplet internal circulation and interface reaction

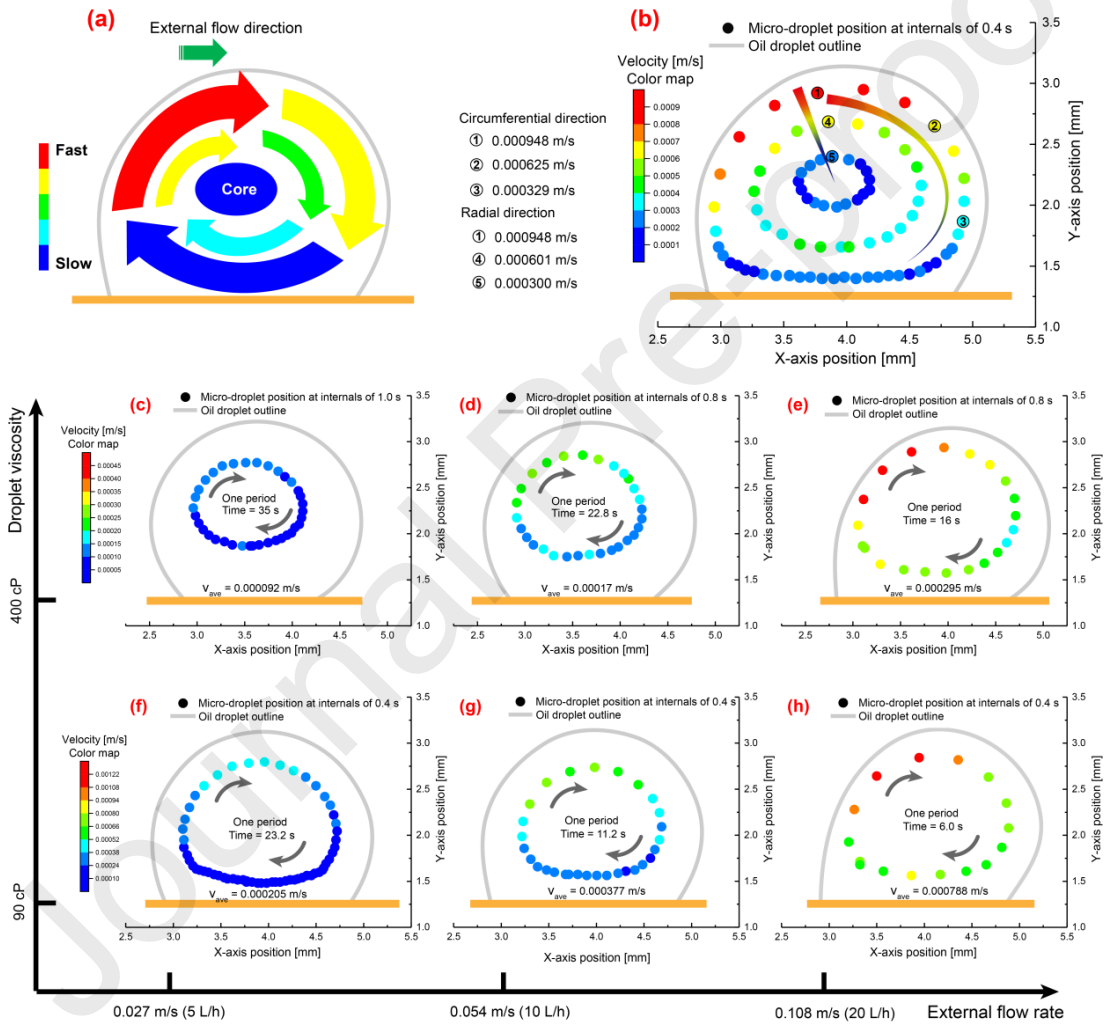

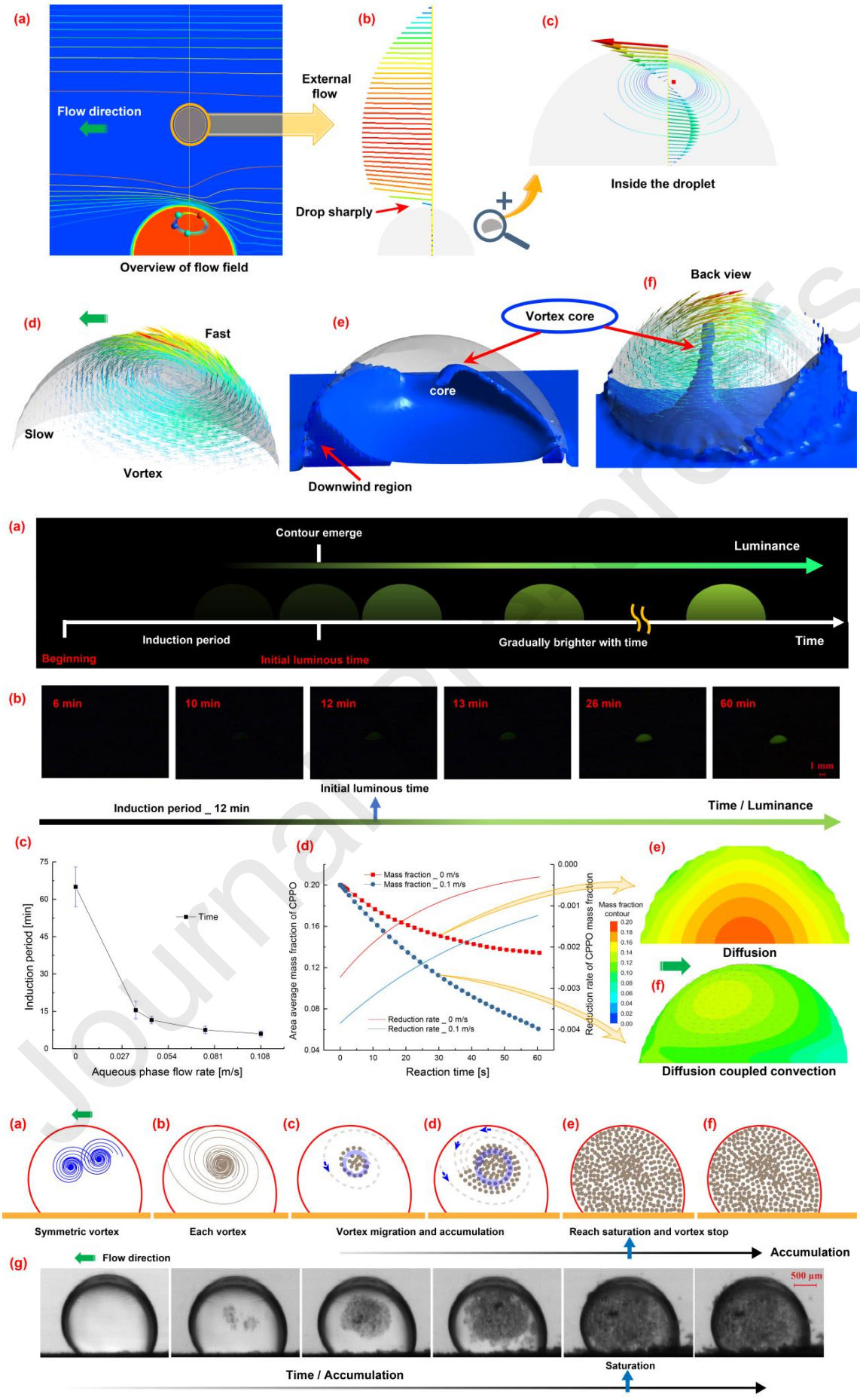
(a)
Flow direction
Overview of flow field
External flow
(b)
Drop sharply
(c)
Inside the droplet
(d)
Fast
Slow
Vortex
(e)
Vortex core
core
Downwind region
(f)
Back view
(a)
Contour emerge
Luminance
Induction period
Beginning
Initial luminous time
Gradually brighter with time
Time
(b)
6 min
10 min
12 min
13 min
26 min
60 min
1 mm
Initial luminous time
Induction period _ 12 min
Time / Luminance
(c)
Induction period [min]
Time
Aqueous phase flow rate [m/s]
(d)
Mass fraction _ 0 m/s
Mass fraction _ 0.1 m/s
Reduction rate _ 0 m/s
Reduction rate _ 0.1 m/s
Area average mass fraction of CPPO
Reduction rate of CPPO mass fraction
Reaction time [s]
(e)
Mass fraction contour
Diffusion
(f)
Diffusion coupled convection
(a)
Symmetric vortex
(b)
Each vortex
(c)
Vortex migration and accumulation
(d)
(e)
Reach saturation and vortex stop
(f)
Accumulation
(g)
Flow direction
500 μm
Saturation
Time / Accumulation